Plasticity of single-atom Pb junctions

M. Müller,[1,*] C. Salgado,[2] N. Néel,[1] J. J. Palacios,[3] and J. Kröger[1,†]
[1]*Institut für Physik, Technische Universität Ilmenau, D-98693 Ilmenau, Germany*
[2]*Departamento de Física de la Materia Condensada, Universidad Autónoma de Madrid, Cantoblanco, E-28049 Madrid, Spain*
[3]*Departamento de Física de la Materia Condensada, Instituto Nicolás Cabrera (INC), and Condensed Matter Physics Center (IFIMAC), Universidad Autónoma de Madrid, Cantoblanco, E-28049 Madrid, Spain*
(Received 30 September 2015; revised manuscript received 9 May 2016; published 1 June 2016)

A low-temperature scanning tunneling microscope was used to fabricate atomic contacts on Pb(111). Conductance characteristics of the junctions were simultaneously recorded with forming and subsequent breaking of the contacts. A pronounced hysteresis effect in conductance traces was observed from junctions comprising the clean Pb(111) surface. The hysteretic behavior was less profound in contacts to single Pb atoms adsorbed to Pb(111). Density-functional calculations reproduced the experimental results by performing a full *ab initio* modeling of plastic junction deformations. A comprehensive description of the experimental findings was achieved by considering different atomic tip apex geometries.

DOI: 10.1103/PhysRevB.93.235402

I. INTRODUCTION

Electrical contacts with constrictions at the atomic scale are receiving substantial attention due to their importance in fundamental and applied sciences [1–3]. In particular, molecular spintronics [4], spin caloritronics [5] and thermoelectric effects in nanoscale junctions [6] are emerging fields. To these investigations, the structural and mechanical properties of the junctions are relevant since electron transport depends crucially on the contact geometry [7,8].

A wealth of experimental and theoretical works have been reported for Au contacts [1], presumably due to their propensity to form monatomic chains bridging the electrodes [9,10]. With appropriate treatment of Au electrodes in break-junction experiments, hysteretic loops were reproducibly observed in conductance-versus-distance traces that were simultaneously recorded with closing and opening of the junctions [11]. This observation was traced to the elasticity of the electrodes. To our knowledge, this work [11] represents the only combination of experimentally observed and theoretically described hysteretic conductance behavior between tunneling and contact range of single-atom junctions that has been available to date. Other materials that have often been used in contact experiments are Ni, Cu, Pd, Ag, Al, and Pt [1]. For some of these materials, conductance hysteresis upon opening high-conductance junctions was reported [12–15].

For Pb contacts, which are the focus of this article, the following experiments and calculations were reported [1]. In an early work, W tips of a scanning tunneling microscope (STM) were approached to Pb(110), and the neck formation was investigated at different sample temperatures [16]. Neck heights exceeding 500 nm were reported, and their growth was rationalized in terms of mobile surface atoms. In another experiment, polycrystalline Pb tips and samples were used to study the conductance of Pb junctions depending on the forces exerted on the electrodes [12]. A jump to contact was observed upon approaching the tip to the sample surface. The resulting junction conductance of less than one quantum of conductance, $G_0 = 2e^2/h$ (e is the elementary charge and h is Planck's constant), was rationalized in terms of constrictions comprising about one atom. In addition, conductance hysteresis was reported after indenting the tip into the substrate, thereby increasing the junction conductance to $\approx 10\ G_0$, and subsequent retraction of the tip. The contact area was appreciably modified by forming asperities with diameters on the order of 100 nm. In a break junction experiment, Pb-Pb contacts were stretched until an abrupt decrease of the conductance occurred from ≈ 1 to 3 G_0 to typical tunneling conductances [17]. Tight-binding calculations assuming a simple pyramid-based geometry for the electrodes confirmed conductance values of $\approx 2.5\ G_0$ as a result of electron transport through sp_z, p_x, and p_y orbitals of the Pb atom bridging the electrodes.

In the ballistic electron transport range, STM experiments revealed that contact formation between Pb-covered W tips and thin films of Pb on Ag(111) depended on the film thickness [18]. While a gradual transition from tunneling to contact was observed for the single Pb wetting layer, the transitions became more abrupt for thicker films. Conductances of contacts comprising the single Pb wetting layer as well as several layers were broadly distributed around $\approx 2\ G_0$. For Pb(111) films on Si(111), atomically resolved conductance traces were obtained by using Pb-coated PtIr tips [19]. On-top, bridge, face-centered-cubic, and hexagonal-close-packed sites of the Pb(111) lattice led to different conductances in the range of ≈ 1–$1.3\ G_0$.

Pb junctions were likewise investigated in electrochemical environments [20]. Accompanying density-functional calculations revealed the importance of the contact geometry for the conductance. In addition, the superconducting properties of Pb contacts exposed to external magnetic fields were demonstrated to depend on the junction geometry [21]. Moreover, atomic Pb wires were grown on a vicinal semiconductor surface and demonstrated to exhibit correlated spin-orbit order [22]. In tunneling junctions comprising Pb electrodes, the competition of superconducting phenomena and Kondo screening [23] as well as tunneling processes into localized subgap states were unraveled [24].

*mueller.m@tu-ilmenau.de
†joerg.kroeger@tu-ilmenau.de

Here, we present a surface science approach to single-atom contacts fabricated from Pb-covered W tips and a Pb(111) surface in a low-temperature STM experiment. The forming and breaking of junctions was performed on pristine Pb(111) as well as on single Pb adsorbed atoms (adatoms). Simultaneously, the conductance of the junction was recorded for tip-sample distances in tunneling and contact ranges. Both types of junctions exhibited a rather broad distribution of contact conductances, i.e., from 1 to 5 G_0 for Pb(111) and from 0.7 to 3 G_0 for Pb adatoms. These variations are not compatible with the previous tight-binding calculations for a single-atom Pb junction where conductance variations from 1 to 2.5 G_0 depending on the distance between the central atom and its first neighbors were reported [25]. In addition, both junctions showed hysteretic behavior. Breaking of the contacts on clean Pb(111) required tip retractions by up to hundreds of pm beyond the jump to contact. Contact regions were imaged prior to and after contact experiments in order to identify surface and tip modifications. The experimental results were corroborated by state-of-the-art *ab initio* quantum-mechanical simulations. The calculations unveiled the important role of relaxations of the tip structure on the contact conductance and the hysteresis width. Atomically sharp and crystalline tips alone were unable to explain the experimental observations. Rather, tip apices terminated by more than one atom had to also be considered to describe the experimentally observed contact conductances and hysteresis effects.

II. EXPERIMENT

The experiments were performed with an STM operated in ultrahigh vacuum (10^{-9} Pa). The absence of the superconducting energy gap in spectra of the differential conductance together with the temperature readings from a Si diode indicated a sample temperature of 7.2–7.5 K. Pb(111) was cleaned by Ar^+ bombardment and annealing. Tips were electrochemically etched from polycrystalline W wire (diameter 300 μm, purity 99.95%) in a 0.1 M solution of NaOH. In the vacuum recipient, the tips were heated close to the W melting temperature. The tip apex was then coated with substrate material by indentation into the Pb(111) surface with an applied voltage of 130 V. A similar procedure was reported previously, which ensured the bulklike character of the Pb coating by measuring the superconducting energy gap [26]. Tip-surface contacts were formed by disabling the feedback loop at a tunneling current of 0.5 nA, in a bias voltage range of 10 mV $\leqslant |V| \leqslant$ 50 mV, and approaching the tip by 300–600 pm toward the surface. The tip approach was stopped a few tens of picometers after the first jump to contact. The tip was then retracted by 1 nm. Approach and retraction velocities ranged between 2 and 3 nm s^{-1}. For the contact experiments, a specific selection of tips was used. The tip was approached to the surface until a single Pb atom was transferred from the tip to the sample upon contact. Atom transfer from the tip apex to the surface was reported previously for several surfaces [2,3,27–29] and is due to the strong adhesive forces between the electrodes close to the point of maximum attraction. Such tips were particularly stable and led to reproducible conductance traces and STM images prior to and after contact formation. STM images were recorded at constant current with the bias voltage applied to the sample. For measurements with a time resolution of 20 ns, a transimpedance amplifier with a 3 dB cutoff frequency of 14 MHz and an oscilloscope sampling rate of 50 MS s^{-1} were used.[1]

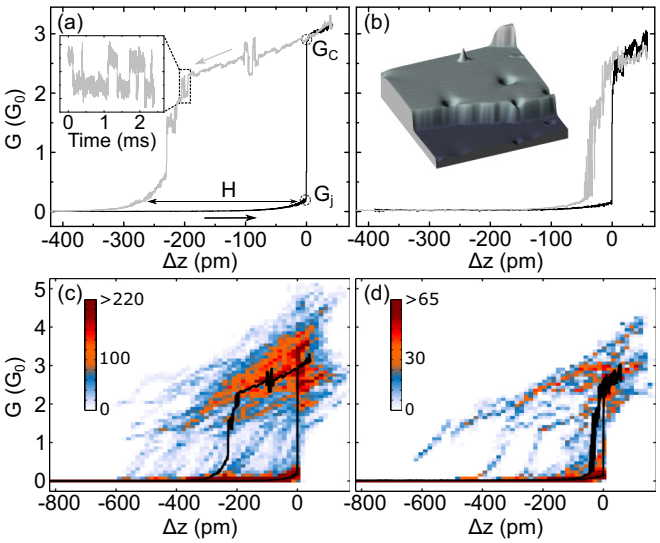

FIG. 1. (a) Representative conductance evolution of a junction comprising Pb(111) and a Pb-coated W tip acquired at 50 mV. Tip approach (black line) leads to an exponential increase of the conductance in the tunneling range (displacements $\Delta z < 0$ pm). The abrupt change of the conductance from $G_j = 0.2$ G_0 to $G_c = 2.9$ G_0 at $\Delta z = 0$ pm reflects the formation of the contact. In the probed contact range ($\Delta z > 0$ pm), the conductance increases linearly. Upon tip retraction (gray line), the conductance decreases linearly and reveals instabilities in the form of, e.g., two-level fluctuations (dashed rectangle). The definition of the hysteresis width, H, is indicated. Inset: two-level fluctuations observed in the conductance trace upon tip retraction. (b) Like (a) for a contact to a single Pb adatom on Pb(111) with $G_j = 0.1$ G_0 and $G_c = 2.2$ G_0. Inset: pseudo-three-dimensional representation of an STM image of Pb(111) (0.1 V, 55 pA, 50 nm × 50 nm). Two terraces are visible. A Pb adatom appears as a protrusion on the upper terrace. Additional structure is due to near-surface voids induced by Ar^+ bombardment [30,31]. Image processing was performed using WSxM [32]. (c),(d) Density plots of all acquired conductance traces [137 for Pb(111), 19 for single Pb adatoms]. The color scale depicts the number of conductance data linearly grouped into bins defined by a regular 90 × 90 grid, which was spanned from −1090 to 260 pm and from 0 to 7 G_0. Full lines are the conductance traces shown in (a) and (b).

III. RESULTS AND DISCUSSION

Tip approach to the clean Pb(111) surface gave rise to the evolution of the junction conductance that is depicted as the black line in Fig. 1(a). The tunneling range in the vicinity of the transition to contact ($-100 < \Delta z < 0$ pm) was characterized by an exponential increase of the conductance with an apparent barrier height of (5.0 ± 0.5) eV. This value is larger than

[1]Experiments were likewise performed with bulk Pb tips. The resulting junctions exhibited virtually identical behavior to the contacts with Pb-covered W tips.

the Pb(111) work function of 4.05 eV [33]. The deviation is in accordance with the previously reported increase of the apparent barrier height close to contact formation on thin Pb films on Ag(111) [18]. Indeed, the calculations presented below revealed strong atomic relaxations in the vicinity of the tunneling-to-contact transition. Therefore, the tip-surface distance decreased faster than the tip displacement, which is defined by a linear voltage ramp applied to the piezoelectric scanning unit.

The transition from the tunneling range to the contact range was reflected by an abrupt increase of the junction conductance. Time-resolved measurements of the jump to contact revealed that the transition was abrupt on a time scale of 20 ns. This almost discontinuous tunneling-to-contact transition was used to define $\Delta z = 0$ pm [Fig. 1(a)]. These observations are compatible with the emerging trend reported previously [18]. While for a single wetting layer of Pb on Ag(111) the transition from the tunneling to the contact range was gradual, it turned into a more abrupt crossover region for thicker Pb films [18]. Therefore, a jump to contact for bulk Pb may be expected and was observed in our experiments. The conductances just before [G_j, Fig. 1(a)] and after (G_c) the jump did not depend on the applied bias voltage in the range of 10 mV $\leqslant |V| \leqslant$ 50 mV. Tunneling spectra of the differential conductance were featureless and nearly constant in that voltage interval.

In the subsequent contact range, i.e., for $\Delta z > 0$ pm, the conductance exhibited a linear increase. Upon tip retraction ($\Delta z < 0$ pm), the junction conductance decreased linearly [gray line in Fig. 1(a)] several hundreds of pm beyond the precedent point of contact formation, i.e., the conductance displayed a pronounced hysteretic behavior. A similar conductance decrease was reported previously and rationalized in terms of the splitting of Pb p orbitals at the Fermi level due to elastic distortions of the contact [25]. During retraction of the tip, two-level fluctuations of the conductance were often observed [dashed rectangle in Fig. 1(a)]. Data acquisition with high time resolution [inset to Fig. 1(a)] revealed that the fluctuations were abrupt changes between two conductance values, which may be attributed to atomic relaxations in the junction [13,34,35]. Local heating of the junction due to power dissipation in the μW range is likely to be present. For Au junctions, a temperature increase of 50 mK was unraveled for this power dissipation [36]. On general grounds, in the case of electron and hole injection into pure metal, a temperature increase on the order of 1 mK may be estimated for the used currents and bias voltages assuming that electrons and holes deposit their energy within the inelastic mean free path [37]. This temperature increase is not sufficient to surpass Ehrlich-Schwoebel barriers (86 meV) [38] and kink energies per atom (61–87 meV) [39] of Pb(111). Therefore, local heating of the junction does not represent the main driving mechanism for the observed junction instabilities. Importantly, after acquiring a typical conductance trace on Pb(111) [Fig. 1(a)], STM images of the contact area showed that in most cases a single atom was transferred from the tip to the surfaces. In less frequent cases, a Pb dimer was transferred.

Contact experiments on single Pb adatoms were likewise performed. Single Pb atoms were transferred from the tip to the Pb(111) surface, as reported previously for other surfaces [2,3,27–29]. The inset to Fig. 1(b) shows an STM image of Pb(111) where a single adatom is visible as a protrusion on the upper terrace. The tip approach to a single Pb adatom exhibited an abrupt change of the conductance at the tunneling-to-contact transition and a linear variation of the conductance in the contact range. A hysteresis loop of the conductance was observed for the adatom, too, albeit considerably less pronounced than on clean Pb(111). A representative example is shown in Fig. 1(b) in which the conductance hysteresis appears with a width of $\approx$50 pm. Imaging the adatom after conductance data acquisition showed that no material had been transferred to the surface.

While the conductance traces in Figs. 1(a) and 1(b) represent specific data sets, Figs. 1(c) and 1(d) comprise all conductance data as density plots. These density plots illustrate the propensity of single-adatom contacts to exhibit smaller conductance hysteresis widths than junctions on clean Pb(111) surfaces. For clarity, the data sets of Figs. 1(a) and 1(b) were added to the density plots as black lines.

Statistics were performed for the contact conductance, G_c, and the hysteresis width, H, in order to more thoroughly compare contact experiments on clean Pb(111) and on single Pb adatoms on Pb(111). Toward that end, G_c was defined as the conductance value that is reached directly after the jump to contact. The hysteresis width was defined as follows [Fig. 1(a)]. A horizontal line starting from G_j—the conductance just before the jump to contact—intersects the conductance trace acquired during retraction. The difference of the corresponding displacements is referred to as H.

Figures 2(a) and 2(b) show histograms of G_c obtained for contacts comprising Pb-covered W tips and the clean Pb(111) surface [Fig. 2(a)] and single Pb adatoms on Pb(111) [Fig. 2(b)]. The distribution of G_c for contacts on Pb(111)

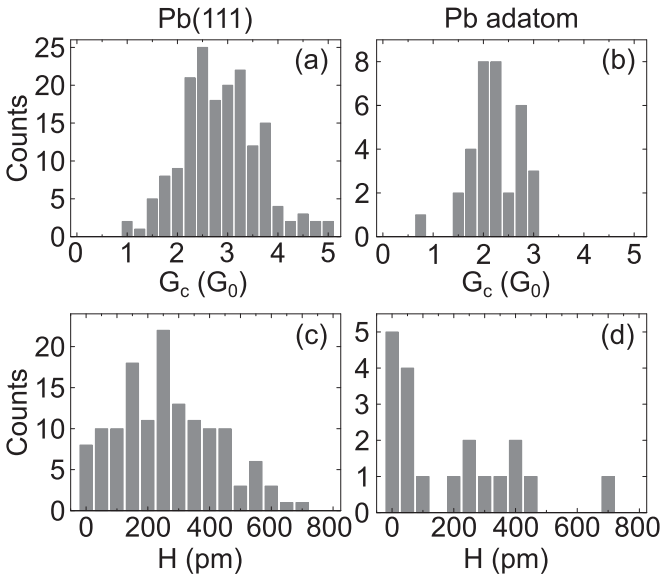

FIG. 2. Histograms of observed contact conductances (G_c) on pristine Pb(111) (a) and on single Pb adatoms (b). (c),(d) Histograms of hysteresis widths (H) observed from closing and subsequent opening of junctions comprising Pb(111) (c) and single Pb adatoms (d). All contacts were formed with bias voltages in the range 10 mV $\leqslant |V| \leqslant$ 50 mV.

TABLE I. Calculated contact conductances (G_c) and hysteresis widths (H) of atom-sized Pb junctions. Pb tips grown in the ⟨100⟩ and ⟨111⟩ directions with apex terminations of $n = 1,4$ and 1,3 atoms, respectively, were considered. On pristine Pb(111), G_c and H were calculated for contacts to on-top and hollow sites. For contacts comprising a Pb adatom, the adatom resided at a Pb(111) hollow site.

Stacking		G_c (G_0)			H (pm)		
direction	n	On-top	Hollow	Adatom	On-top	Hollow	Adatom
⟨100⟩	1	0.7	0.9	0.9	270	180	40
	4	2.2	4.5	2.2	200	140	260
⟨111⟩	1	1.5	2.2	1.2	150	410	110
	3	2.4	2.3	2.4	480	530	480

exhibited a broad maximum at ≈2.5 G_0. Contacts on three-layer-thick Pb films on Ag(111) were previously reported to exhibit similar conductances [18]. However, these contact conductances were observed less frequently than contact conductances of ≈1.4 G_0 [18]. Junctions comprising a single Pb adatom showed a maximum in the histogram of G_c that is more sharply peaked between 2 and 2.25 G_0. The different widths of the conductance histograms are assigned to the degree of precise knowledge of the contact geometry. The Pb(111) surface was not imaged with atomic resolution. Therefore, whether contact was formed to on-top, hollow, or bridge lattice sites of Pb(111) remained elusive. In contrast, contact to the adatom left less doubt as to the junction geometry at the substrate, and thus it led to a sharper distribution of G_c. These findings are in agreement with results obtained for Ag(111), Cu(111) [27], and Au(111) [28,29]. Below, we will show that contact conductances calculated for different lattice sites and tip geometries corroborate the experimental results (Table I).

Histograms of the hysteresis widths are different for Pb(111) [Fig. 2(c)] and Pb adatoms [Fig. 2(d)], too. For contacts on clean Pb(111), the distribution is broad with a maximum at ≈250 pm. Junctions comprising Pb adatoms most frequently exhibit conductance hysteresis widths between 0 and 50 pm. In the probed bias voltage range 10 mV $\leqslant |V| \leqslant$ 50 mV and within the uncertainty margins, the hysteresis width did not depend on the sample voltage. Moreover, the potential influence of Pb phonons was not explored since bulk and surface phonon energies are below 10 meV [40].

For both contact types, breaking of the junctions was accompanied by conductance instabilities before the jump out of contact occurred. These findings are different from results reported for Au contacts [11]. The hysteretic conductance variations in Au contacts were characterized by clear jumps to contact and jumps out of contact. Stretching of the Au junctions led to a gradual decrease of the conductance without the occurrence of conductance fluctuations. These observations were rationalized in terms of junctions in which no further atomic reorganizations took place, i.e., the closing and opening of the Au contacts was understood by elastic deformations of the electrodes [11]. For Pb, however, our *ab initio* quantum-mechanical calculations showed that reorganizations of the electrode structure occurred, i.e., the junctions were characterized by plastic deformations. In particular, several atoms were involved in forming and breaking the contact. This interpretation is compatible with our observation that the hysteresis width increased slightly with increasing contact conductance (not shown).

To rationalize the experimental data and gain insight into the relation between the mechanical or structural properties and the conductance of the contacts, a full set of density-functional calculations was performed. While it is common practice to address the mechanical behavior of contacts at the nanometer scale through molecular dynamics and effective interatomic potentials [41], the detailed and controlled nature of the present experiments called for taking quantum effects on the forces into account. Both the mechanical behavior and the electron transport were addressed by means of our code ANT.G [42,43] in combination with GAUSSIAN [44]. The atomic and electronic structure of the relevant contact region were obtained in a fully self-consistent manner and translated into a conductance through a standard Green function formalism with the help of effective self-energies representing the far and less relevant part of the system [42,43,45,46]. To expand the electronic density and represent the Green function, the CRENBS minimal basis set was typically used, with one s and three p orbitals, including its corresponding core pseudopotentials [47]. Additionally, calculations with larger basis sets such as the LANL2DZ were performed [48]. However, the resulting atomic and electronic properties were virtually identical to the findings obtained by the minimal basis sets. Tight-binding calculations of the electronic structure for the same geometries led to similar results. A standard local density approximation to the density functional was used. The choice of the functional is not critical to the results for monoelemental *sp* metals. The specific procedure to mimic the experiments involved successive instantaneous structural relaxations subject to certain geometrical constraints on the boundary atoms of our system, which coupled to the bulk substrate and the rest of the tip.

The geometry of the surface and of the contact was known to a very good extent due to the imaging capabilities of the STM. However, to reduce the large number of possible atomic coordinates, the starting atomic structure of the tip prior to contact had in part to be guessed. For all calculations, Pb tips grown in the ⟨100⟩ and ⟨111⟩ directions were chosen. This choice was motivated by the findings of several previous works. Pb tips grown along the ⟨100⟩ and ⟨111⟩ directions exhibit {111} facets, which were shown to exhibit the lowest surface energy [49]. Face-centered-cubic metals in general realize ⟨100⟩ and ⟨111⟩ stacking directions, which was demonstrated for, e.g., Au [9,50–52], Pt [52], and Al [53] electrodes. Consequently, four obvious choices for the tip termination were available, i.e., the commonly assumed single-atom termination for both orientations and a termination via a four-atom or three-atom plane parallel to the surface for tips grown in the ⟨100⟩ and ⟨111⟩ direction, respectively. While these choices did not cover all possible configurations, the particular preparation of the tip (*vide supra*) certainly reduced the number of possibilities. The clean Pb(111) surface was represented by an embedded three-layer cluster of up to 100 atoms. The calculations revealed that hexagonal-close-packed hollow sites of Pb(111) represent energetically favored adsorption sites for single Pb atoms.

Comparing calculated G_c for ⟨100⟩ and ⟨111⟩ tips (Table I), similar values were found. A notable exception is $G_c = 2.2$ G_0 obtained for single-atom terminated ⟨111⟩ tips at Pb(111) hollow sites. This elevated conductance may tentatively be ascribed to the particular junction geometry where the tip continues the stacking of the sample. This situation may maximize the transmission of transport channels. We further found that ⟨111⟩ tips exhibited larger hysteresis widths than ⟨100⟩ tips. Due to the larger surface-to-volume ratio of ⟨111⟩ tips, fewer bonds need to be broken in the course of plastic deformations. Therefore, ⟨111⟩ tips may be considered less stiff than ⟨100⟩ tips, which favors more pronounced hysteresis effects. Apart from this, Table I reflects the fact that ⟨100⟩ and ⟨111⟩ tips exhibit similar trends. Consequently, we will concentrate on the findings obtained for ⟨100⟩ tips in the following.

Entire conductance traces were calculated for tips approaching and retracting from on-top and hollow sites of the pristine Pb(111) surface as well as Pb adatoms. Representative data obtained for ⟨100⟩ tips are shown in Figs. 3(a) and 3(e) for Pb(111) and in Figs. 3(b) and 3(f) for Pb adatoms. Additionally, conductance traces for single Pb adatoms [Figs. 3(b) and 3(f)] were simulated. The orientation of the tip structure with respect to the Pb(111) lattice is indicated for the single-atom [Figs. 3(c) and 3(d)] and the four-atom [Figs. 3(g) and 3(h)] terminated tip. In the calculations, contact formation ($\Delta z = 0$ pm) was defined by a conductance increase exceeding 0.3 G_0 between two subsequent tip displacements. An additional requirement was the variation of the conductance by less than 0.3 G_0 for two subsequent displacements in the contact range ($\Delta z >$ 0 pm). According to this definition, the single-atom terminated Pb tip exhibited calculated contact conductances of $G_c = 0.7$ and 0.9 G_0 for on-top and hollow sites on Pb(111), respectively [Fig. 3(a)]. The geometry of such low-conductance junctions is depicted in Fig. 3(i) for the on-top configuration at displacement $\Delta z = 0$ pm. Distortions of the tip and the substrate were still elastic at this displacement. In particular, the tip apex atom was centered atop the approached Pb(111) atom. The calculations unveiled that the geometry of these low-conductance junctions was unstable. Indeed, the simulations revealed that these junctions exhibited the propensity for atomic relaxations upon further tip approach. Approaching the single-atom terminated tip toward the Pb(111) on-top (hollow) site by 140 pm (60 pm) led to a strong increase of the junction conductance, rather than to a plateaulike variation. The calculated junction geometry showed the implantation of the tip apex atom into the surface [Fig. 3(i), $\Delta z = 220$ pm], which caused the conductance increase.

Forming and breaking of contacts comprising a single-atom terminated tip and the pristine Pb(111) surface revealed hysteretic behavior [Fig. 3(a)]. The hysteresis widths were extracted from calculated conductance traces according to the procedure exposed in Fig. 1(a). For single-atom terminated tips, hysteresis widths of 270 and 180 pm were obtained for on-top and hollow sites, respectively (Table I). Figure 3(i) further shows that single-atom terminated tips transfer their apex atom to the bare Pb(111) surface upon contact, in agreement with the experimental observation. Upon approaching a Pb(111) on-top site, the tip apex atom was transferred to an adjacent hollow site upon contact, reflecting the preferred adsorption site of a single Pb atom.

Junctions comprising an atomically sharp tip and a single Pb adatom showed the conductance-displacement characteristics depicted in Fig. 3(b). In contrast to the simulation of contacts comprising the pristine Pb(111) surface, a nearly gradual evolution of the conductance in the transition range between tunneling an contact was observed, rather than an abrupt jump. The contact conductance was ≈0.9 G_0 and thus appreciably lower than the averaged experimental value. Only a few contacts were experimentally observed with a similarly low conductance [Fig. 2(b)]. In addition, a conductance

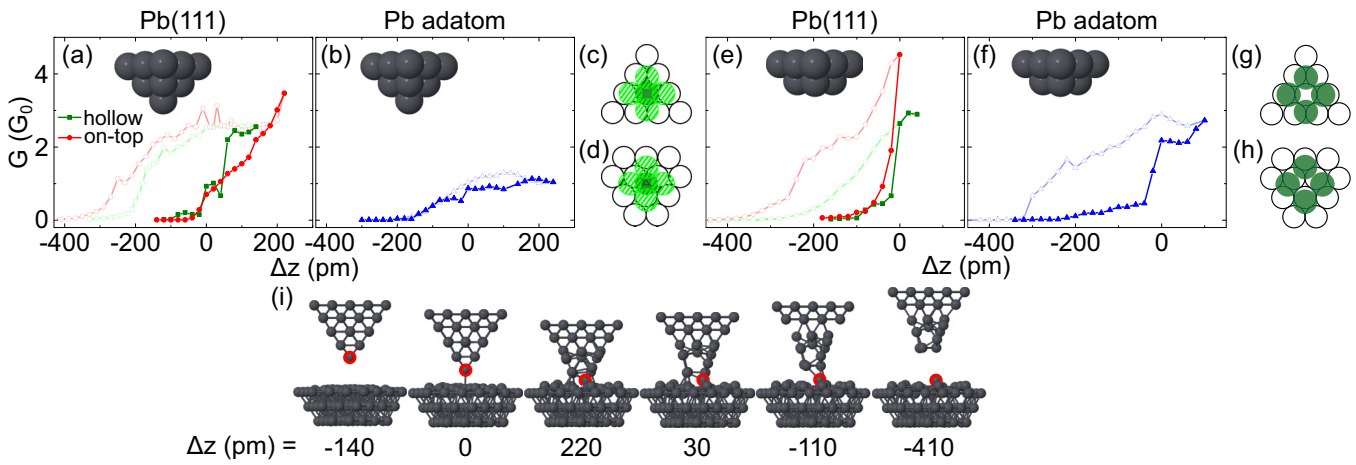

FIG. 3. Calculation of conductance-distance characteristics for forming and breaking Pb contacts with a tip grown along the ⟨100⟩ direction. (a) A single-atom terminated tip approaches (filled symbols) and retracts from (open symbols) on-top (squares) and hollow (circles) Pb(111) lattice sites. (b) Same as (a) for a single Pb adatom (triangles). (c),(d) Position of single-atom terminated tip (filled and hatched circles for an apex atom and second-layer atoms, respectively) relative to the Pb(111) lattice (circles) for contacts comprising the on-top (c) and the hollow (d) site. (e),(f) Like (a),(b) for a four-atom terminated tip. (g),(h) Position of four-atom terminated tip (filled circles) relative to the Pb(111) lattice (circles) for contacts comprising the on-top (g) and hollow (h) site. (i) Snapshots of calculated contact geometries for a single-atom terminated tip approaching an on-top site of pristine Pb(111). Increasing (decreasing) displacements (Δz) correspond to the tip approach (retraction). Upon retraction, the tip apex atom (encircled by a full red line) is transferred to a Pb(111) hollow site adjacent to the approached on-top site.

hysteresis was virtually absent for the simulated contacts to adatoms.

The broad range of contact conductances observed in the experiments, i.e., ≈1.0 to ≈5.0 G_0 for Pb(111) and ≈0.7 to ≈3 G_0 for Pb adatoms, could not be explained by tip apices terminated by a single atom alone. According to Table I, calculated contact conductances comprising single-atom terminated ⟨100⟩ and ⟨111⟩ tips and on-top and hollow sites of Pb(111) range from 0.7 to 2.2 G_0, respectively, while contacts to a single Pb adatom exhibit a conductance range spanning 0.9–1.2 G_0. These deviations to experimental observations represented the impetus to likewise consider junctions comprising tips terminated by more than a single Pb atom in the simulations.

Representative conductance-displacement characteristics are displayed in Fig. 3(e) for contacts of ⟨100⟩ tips at on-top and hollow Pb(111) sites and in Fig. 3(f) for single Pb adatoms residing at Pb(111) hollow sites. In agreement with the experiment, abrupt changes of tunneling to contact conductances and jumps out of contact occurred in the calculations. The calculated contact conductance for on-top and hollow Pb(111) sites was 2.2 and 4.5 G_0, respectively.[2] Contacts comprising a four-atom terminated tip and a single Pb adatom exhibited a conductance of 2.2 G_0. The calculated hysteresis widths were 200 and 140 pm for on-top and hollow sites of Pb(111), respectively, and 260 pm for the Pb adatom. The simulated hysteresis width for the adatom junction exceeds the experimentally most frequently observed widths between 0 and 50 pm [Fig. 2(d)]. A few junctions exhibited hysteresis widths in the range of 200–450 pm, which are compatible with the calculated result, in particular when ⟨111⟩ tips are considered (Table I). For the other ideal contact geometry considered in the calculations, i.e., a single-atom terminated tip and the adatom, an essentially vanishing H was obtained [Fig. 3(b)]. Therefore, the experimental junction most likely adopts a geometry within the range of these two extreme and ideal cases. Unlike the simulations based on a single-atom terminated tip, the approach of a four-atom terminated tip to a single Pb adatom on Pb(111) [Fig. 3(f)] showed—in accordance with the experiment—an abrupt jump to and out of contact. Therefore, considering both single-atom and four-atom terminated tips in the simulations led to an improved description of the broad conductance distribution observed in the experiments. Furthermore, the conductance hysteresis observed from closing and opening the junctions was well reproduced.

[2]Calculations revealed that contacts comprising a four-atom terminated tip apex and on-top sites of Pb(111) involved many atoms in the contact range. In particular, decreasing the tip-surface distance led to an increase of the conductance without reaching a plateaulike conductance variation. Therefore, for this specific junction geometry, contact was defined at the same displacement Δz at which contact was reached for junctions comprising four-atom terminated tips and Pb(111) hollow sites.

IV. CONCLUSION

Closing tunneling junctions comprising Pb tips of an STM and Pb(111) surfaces occurred via an abrupt jump to the first ballistic-conductance plateau. Upon opening such junctions, a pronounced hysteretic conductance behavior was observed. In contrast to previously studied Au junctions, the Pb conductance hysteresis was not solely due to elastic distortions of the electrodes. Rather, it reflected the plasticity of Pb constrictions even at the ultimate size limit. Additionally, to comprehensively describe electron transport through the biased Pb contacts and mechanical relaxations of the junctions, simulations had to deviate from the commonly assumed simple pyramidal tip structure and include more complex tip apices that were terminated by more than a single atom. The presented findings, therefore, highlight the fact that low-conductance junctions do not necessarily reflect simple junction geometries. Moreover, the results are relevant to mechanical deformations at the nanometer scale.

ACKNOWLEDGMENTS

Financial support by the Carl Zeiss Foundation is acknowledged. This work was supported by MINECO under Grant No. FIS2013-47328-C01, by European Union structural funds and the Comunidad de Madrid Program S2013/MIT-2850, and by Generalitat Valenciana under Grant No. PROMETEO/2012/011. The authors acknowledge the computer resources, technical expertise, and assistance provided by the Centro de Computacion Científica of the Universidad Autónoma de Madrid.

[1] N. Agraït, A. L. Yeyati, and J. M. van Ruitenbeek, Phys. Rep. **377**, 81 (2003).
[2] J. Kröger, N. Néel, and L. Limot, J. Phys. Condens. Matter **20**, 223001 (2008).
[3] R. Berndt, J. Kröger, N. Néel, and G. Schull, Phys. Chem. Chem. Phys. **12**, 1022 (2010).
[4] S. Sanvito, Chem. Soc. Rev. **40**, 3336 (2011).
[5] G. E. W. Bauer, E. Saitph, and B. J. van Wees, Nat. Mater. **11**, 391 (2012).
[6] Y. Dubi and M. Di Ventra, Rev. Mod. Phys. **83**, 131 (2011).
[7] Y. F. Wang, J. Kröger, R. Berndt, H. Vázquez, M. Brandbyge, and M. Paulsson, Phys. Rev. Lett. **104**, 176802 (2010).
[8] G. Schull, T. Frederiksen, A. Arnau, D. Sánchez-Portal, and R. Berndt, Nat. Nanotechnol. **6**, 23 (2011).
[9] H. Ohnishi, Y. Kondo, and K. Takayanagi, Nature (London) **395**, 780 (1998).
[10] A. I. Yanson, G. R. Bollinger, H. E. van den Brom, N. Agraït, and J. M. van Ruitenbeek, Nature (London) **395**, 783 (1998).
[11] M. L. Trouwborst, E. H. Huisman, F. L. Bakker, S. J. van der Molen, and B. J. van Wees, Phys. Rev. Lett. **100**, 175502 (2008).

[12] N. Agraït, J. G. Rodrigo, G. Rubio, C. Sirvent, and S. Vieira, Thin Solid Films **253**, 199 (1994).
[13] H. E. den Brom, A. I. Yanson, and J. M. van Ruitenbeek, Physica B **252**, 69 (1998).
[14] A. Halbritter, S. Csonka, O. Y. Kolesnychenko, G. Mihály, O. I. Shklyarevskii, and H. van Kempen, Phys. Rev. B **65**, 045413 (2002).
[15] J. G. Rodrigo, H. Suderow, S. Vieira, E. Bascones, and F. Guinea, J. Phys. Condens. Matter **16**, R1151 (2004).
[16] L. Kuipers and J. W. M. Frenken, Phys. Rev. Lett. **70**, 3907 (1993).
[17] E. Scheer, N. Agraït, J. C. Cuevas, A. L. Yeyati, B. Ludoph, A. Martín-Rodero, G. R. Bollinger, J. M. van Ruitenbeek, and C. Urbina, Nature (London) **394**, 154 (1998).
[18] M. Becker and R. Berndt, New J. Phys. **12**, 113010 (2010).
[19] H. Kim and Y. Hasegawa, Phys. Rev. Lett. **114**, 206801 (2015).
[20] F.-Q. Xie, F. Hüser, F. Pauly, C. Obermair, G. Schön, and T. Schimmel, Phys. Rev. B **82**, 075417 (2010).
[21] J. G. Rodrigo, V. Crespo, H. Suderow, S. Vieira, and F. Guinea, Phys. Rev. Lett. **109**, 237003 (2012).
[22] C. Brand, H. Pfnür, G. Landolt, S. Muff, J. H. Dil, T. Das, and C. Tegenkamp, Nat. Commun. **6**, 8118 (2015).
[23] K. J. Franke, G. Schulze, and J. I. Pascual, Science **332**, 940 (2011).
[24] M. Ruby, F. Pientka, Y. Peng, F. von Oppen, B. W. Heinrich, and K. J. Franke, Phys. Rev. Lett. **115**, 087001 (2015).
[25] J. C. Cuevas, A. Levy Yeyati, A. Martín-Rodero, G. R. Bollinger, C. Untiedt, and N. Agraït, Phys. Rev. Lett. **81**, 2990 (1998).
[26] M. Ruby, B. W. Heinrich, J. I. Pascual, and K. J. Franke, Phys. Rev. Lett. **114**, 157001 (2015).
[27] L. Limot, J. Kröger, R. Berndt, A. Garcia-Lekue, and W. A. Hofer, Phys. Rev. Lett. **94**, 126102 (2005).
[28] J. Kröger, H. Jensen, and R. Berndt, New J. Phys. **9**, 153 (2007).
[29] J. Kröger, N. Néel, A. Sperl, Y. Wang, and R. Berndt, New J. Phys. **11**, 125006 (2009).
[30] M. Schmid, W. Hebenstreit, P. Varga, and S. Crampin, Phys. Rev. Lett. **76**, 2298 (1996).
[31] O. Kurnosikov, O. A. O. Adam, H. J. M. Swagten, W. J. M. de Jonge, and B. Koopmans, Phys. Rev. B **77**, 125429 (2008).
[32] I. Horcas, R. Fernández, J. M. Gómez-Rodríguez, J. Colchero, J. Gómez-Herrero, and A. M. Baro, Rev. Sci. Instrum. **78**, 013705 (2007).
[33] K. Jacobi, Phys. Rev. B **38**, 5869 (1988).
[34] A. Sperl, J. Kröger, and R. Berndt, Phys. Rev. B **81**, 035406 (2010).
[35] N. Néel, J. Kröger, and R. Berndt, Nano Lett. **11**, 3593 (2011).
[36] W. Lee, K. Kim, W. Jeong, L. A. Zotti, F. Pauly, J. C. Cuevas, and P. Reddy, Nature (London) **498**, 209 (2013).
[37] F. Flores, P. M. Echenique, and R. H. Ritchie, Phys. Rev. B **34**, 2899 (1986).
[38] S.-C. Li, Y. Han, J.-F. Jia, Q.-K. Xue, and F. Liu, Phys. Rev. B **74**, 195428 (2006).
[39] K. Arenhold, S. Surnev, H. P. Bonzel, and P. Wynblatt, Surf. Sci. **424**, 271 (1999).
[40] I. Y. Sklyadneva, R. Heid, K.-P. Bohnen, P. M. Echenique, and E. V. Chulkov, J. Phys. Condens. Matter **24**, 104004 (2012).
[41] C. Sabater, C. Untiedt, J. J. Palacios, and M. J. Caturla, Phys. Rev. Lett. **108**, 205502 (2012).
[42] J. J. Palacios, A. J. Pérez-Jiménez, E. Louis, E. SanFabián, and J. A. Vergés, Phys. Rev. B **66**, 035322 (2002).
[43] E. Louis, J. A. Vergés, J. J. Palacios, A. J. Pérez-Jiménez, and E. SanFabián, Phys. Rev. B **67**, 155321 (2003).
[44] M. J. Frisch, G. W. Trucks, H. B. Schlegel, G. E. Scuseria, M. A. Robb, J. R. Cheeseman, G. Scalmani, V. Barone, B. Mennucci, G. A. Petersson, H. Nakatsuji, M. Caricato, X. Li, H. P. Hratchian, A. F. Izmaylov, J. Bloino, G. Zheng, J. L. Sonnenberg, M. Hada, M. Ehara, K. Toyota, R. Fukuda, J. Hasegawa, M. Ishida, T. Nakajima, Y. Honda, O. Kitao, H. Nakai, T. Vreven, J. A. Montgomery, Jr., J. E. Peralta, F. Ogliaro, M. Bearpark, J. J. Heyd, E. Brothers, K. N. Kudin, V. N. Staroverov, R. Kobayashi, J. Normand, K. Raghavachari, A. Rendell, J. C. Burant, S. S. Iyengar, J. Tomasi, M. Cossi, N. Rega, J. M. Millam, M. Klene, J. E. Knox, J. B. Cross, V. Bakken, C. Adamo, J. Jaramillo, R. Gomperts, R. E. Stratmann, O. Yazyev, A. J. Austin, R. Cammi, C. Pomelli, J. W. Ochterski, R. L. Martin, K. Morokuma, V. G. Zakrzewski, G. A. Voth, P. Salvador, J. J. Dannenberg, S. Dapprich, A. D. Daniels, Ö. Farkas, J. B. Foresman, J. V. Ortiz, J. Cioslowski, and D. J. Fox, *Gaussian 09, Revision D.01* (Gaussian, Inc., Wallingford CT, 2009).
[45] J. J. Palacios, A. J. Pérez-Jiménez, E. Louis, and J. A. Vergés, Phys. Rev. B **64**, 115411 (2001).
[46] D. Jacob and J. J. Palacios, J. Chem. Phys. **134**, 044118 (2011).
[47] R. B. Ross, J. M. Powers, T. Atashroo, W. C. Ermler, L. A. LaJohn, and P. A. Christiansen, J. Chem. Phys. **93**, 6654 (1990).
[48] W. R. Wadt and P. J. Hay, J. Chem. Phys. **82**, 284 (1985).
[49] J.-M. Zhang, F. Ma, and K.-W. Xu, Appl. Surf. Sci. **229**, 34 (2004).
[50] V. Rodrigues, T. Fuhrer, and D. Ugarte, Phys. Rev. Lett. **85**, 4124 (2000).
[51] L. G. C. Rego, A. R. Rocha, V. Rodrigues, and D. Ugarte, Phys. Rev. B **67**, 045412 (2003).
[52] C. Evangeli, M. Matt, L. Rincón-García, F. Pauly, P. Nielaba, G. Rubio-Bollinger, J. C. Cuevas, and N. Agraït, Nano Lett. **15**, 1006 (2015).
[53] C. Schirm, M. Matt, F. Pauly, J. C. Cuevas, P. Nielaba, and E. Scheer, Nat. Nanotechnol. **8**, 645 (2013).